Journal of Wasit for Science and Medicine 2026:19, (4), 76-80

Core-Separation Control of Supermode Splitting and Coupling Dynamics in Symmetric Dual-Core Optical Fibers

Eidan A. Abdullah
Department of Physics, College of Science, University of Wasit, Wasit, Iraq
eidan@uowasit.edu.iq

Abstract

The effect of core separation on supermode splitting and optical power exchange was studied in a symmetric step-index dual-core fiber. A scalar finite-difference eigensolver was used to compute the propagation constants of the fundamental even and odd supermodes. A separate split-step Fourier beam-propagation calculation (BPM) was used to simulate the propagation of a Gaussian beam launched into one core. For a fixed wavelength of 1.55 μm, the separation between the cores was varied from 6 to 9 μm, while the other structural parameters remained unchanged. As the cores were separated, their effective-index splitting decreased, and the first predicted transfer length increased from approximately 0.5 to 4.4 mm. At the four separations considered, the BPM transfer maxima were within 1% of the supermode estimates. The longitudinal intensity maps indicated more frequent power exchange at smaller separations and slower oscillations at larger separations. This numerical agreement provides a consistency check between the two scalar calculations. It does not establish experimental accuracy or full-vector performance.

Keywords: dual-core optical fiber; supermodes; evanescent coupling; coupled-mode theory; beam propagation method; coupling length.

1. Introduction

A number of cores can be used for the same light. Allowing common fiber cladding, independent spatial channels to be carried in. one structure. This is "this is that" style. Has been used to broadcast digital data. also found applications in interferometric applications of and distributed sensing, quantum, and the word communication and nonlinear optical. devices [6–9]. Coupling between adjacent cores may be desirable or undesirable, depending on the device: it generates crosstalk in transmission link, but gives a better value of controlled power exchange needed in a directional coupler [10–12]. The basic coupling mechanism is readily illustrated by a pair of identical cores. Each

isolated-core mode extends beyond its core boundary, so the evanescent tails overlap when the cores are sufficiently close. The coupled structure then supports fundamental even and odd supermodes rather than independent single-core eigenmodes. Excitation near one core generally produces a superposition of these two states. Because they have different propagation constants, relative phase changes as a function of distance and the optical power are redistributed on a regular basis. between the cores.

The relation between the transfer length of the supermodes is constructed in a dielectric-waveguide.Coupled-mode theory (CMT) [10–16]. The fields which overlap are guided. Especially susceptible to core separation. At smaller spacing, the difference between the larger the propagation constant is for even and odd modes and power transmission takes place over a shorter distance.

The further apart the mouse is, the less of both these effects will occur. This is a deliberate act when using fiber must be controlled when intercore crosstalk is not desired [17-20] couplers.Spacing by itself, however, is not a complete design specification: the core radius, index contrast, wavelength, and launch field all affect the interpretation of a measured or simulated transfer length.

Contemporary dual-core devices are not restricted to identical circular step-index cores. Photonic-crystal, asymmetric, all-solid, and hollow-core designs have been examined for polarization control, nonlinear switching, and ultrafast or wavelength-selective operation [21–24]. Dual-core fibers are also incorporated into grating-based and surface-plasmon-resonance sensors [25–27]. These examples motivate accurate modeling of inter-core interaction. At the same time, their additional structural and vectorial effects make direct comparisons with a simple scalar model inappropriate.

Two standard calculations describe different aspects of this problem. An eigenmode solver gives the propagation constants of the coupled fiber and, hence, the ideal beating length. Beam-propagation methods (BPM) start instead from an imposed field and show where power is found as the beam evolves. Both have an established place in guided-wave modeling [10–16,28–30], including studies of coupling in dual-core structures [31–33]. A Gaussian launched into one core is not necessarily an equal mixture of only the two fundamental supermodes. Furthermore, a transverse Helmholtz eigensolver and paraxial BPM do not make identical approximations. It is useful, therefore, to compare the beating length with the transfer peaks obtained by propagation for exactly the same index profile.

In this comparison, the fiber geometry was held fixed apart from the center separation, which was set to 6, 7, 8, and 9 μm. These points were selected so that power exchange could be followed within a 10 mm computational interval; they are not manufacturing limits or optimized spacings. For each separation, the fundamental supermode pair was calculated, its index splitting evaluated, and the first inter-core transfer maximum located from BPM. The result is a numerical comparison for this particular geometry and excitation.

2. Numerical model and procedure

2.1. Dual-core geometry

Two identical circular step-index cores were placed in a uniform cladding. Their centers were specified by (x, y) = (±d/2, 0), where d denotes the center separation. The core radius was a = 2.5 μm, and the wavelength was λ = 1.55 μm. The refractive indices were n_{core} = 1.461 and n_{clad} = 1.443. Calculations were made for d = 6, 7, 8, and 9 μm. The indicator function $\chi_{core}(x,y)$ equals one inside either core disk, $(x \pm d/2)^2 + y^2 \leq a^2$, and zero elsewhere. The index profile is consequently

$$n(x,y) = n_{\text{clad}} + \delta n\, \chi_{\text{core}}(x,y) \qquad \delta n = n_{\text{core}} - n_{\text{clad}} \tag{1}$$

The transverse index profile was kept uniform along the propagation direction. Absorption, bending, longitudinal perturbations, nonlinear effects, and wavelength dispersion were not included. Polarization splitting and full-vector field conditions at material interfaces are likewise outside the scalar weak-guidance approximation used here [10–12]. The specific question addressed here is whether supermode splitting and BPM yield consistent coupling lengths for the same dual-core geometry as the core separation changes.

2.2. Finite-difference supermodes

For each separation, the scalar transverse Helmholtz eigenvalue problem was solved with $k_0 = 2\pi/\lambda$:

$$\mathcal{H}_\perp \psi_m = \beta_m^2 \psi_m \qquad \mathcal{H}_\perp = \nabla_\perp^2 + k_0^2 n^2(x,y) \tag{2}$$

The effective index associated with mode m is

$$n_{\text{eff},m} = \frac{\beta_m}{k_0} \tag{3}$$

The transverse domain extended from −62.5 to +62.5 μm on both axes. A 401 × 401 grid gives Δx = Δy = 0.3125 μm. Second-order central differences were applied to the transverse derivatives, and homogeneous Dirichlet conditions were imposed at the outer boundaries. From the guided solutions with the highest effective indices, the fundamental pair is selected using eigenvalue ordering and the expected symmetry: $\psi_{even}(-x,y) = \psi_{even}(x,y)$ and $\psi_{odd}(-x,y) = -\psi_{odd}(x,y)$. The resulting fields for d = 8 μm appear in Fig. 1.

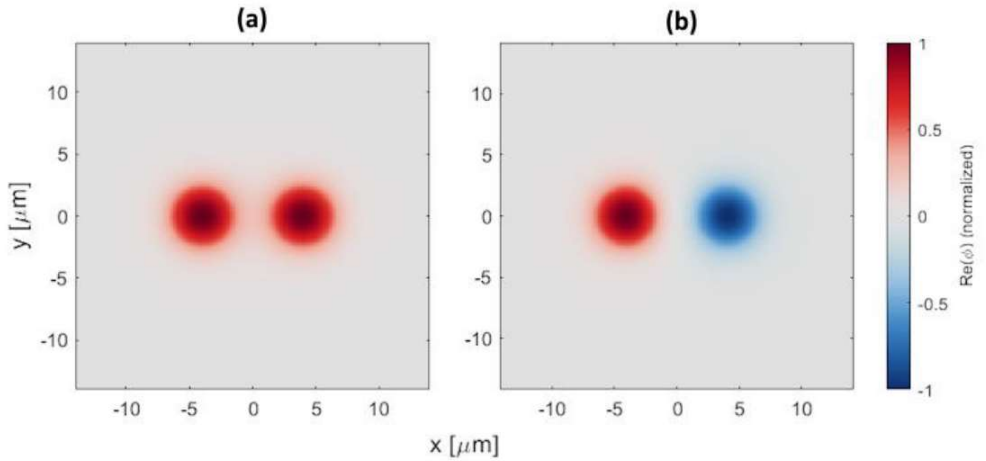


Figure 1. Normalized real parts of the fundamental supermodes at d = 8 μm: (a) even and (b) odd.

2.3. Modal splitting and coupling length

The effective-index difference between the two fundamental supermodes is defined as

$$\Delta n_{\text{eff}} = n_{\text{eff,even}} - n_{\text{eff,odd}} \quad (4)$$

A nearly balanced excitation of the even and odd supermodes transfers power ideally when their relative phase first reaches π. The corresponding transfer length is

$$L_{c,\text{CMT}} = \frac{\pi}{\Delta\beta} = \frac{\lambda}{2\Delta n_{\text{eff}}} \quad (5)$$

$$\Delta\beta = \beta_{\text{even}} - \beta_{\text{odd}}$$

For a symmetric coupler, Eq. (5) is the transfer length expected from the beating of its fundamental even and odd supermodes [13–16]. Their sum can concentrate the field in one core, whereas their difference concentrates it in the other. Propagation changes the relative phase of the two contributions and therefore shifts the intensity between cores. This construction describes ideal two-mode exchange, not the efficiency of coupling an arbitrary incident beam into guided states. The propagation constants used here come directly from the finite-difference eigenvalue calculation; an overlap-integral coupling coefficient was not evaluated separately.

2.4. Beam propagation calculation

For a direct calculation of the longitudinal field, scalar split-step Fourier BPM was used with a Gaussian input centered on the left core:

$$A(x, y, 0) = A_0 \exp\left[-\frac{\rho^2}{w_0^2}\right] \quad (6)$$

$$\rho^2 = (x + d/2)^2 + y^2$$

The beam waist is $w_0 = 0.85a = 2.125$ μm. The amplitude A_0 was selected to normalize the initial transverse power to unity. The propagation equation in the scalar paraxial approximation is

$$\frac{\partial A}{\partial z} = \frac{i}{2k_{\mathrm{ref}}}\mathcal{D}A$$
$$\mathcal{D} = \nabla_{\perp}^{2} + k_0^2 n^2(x,y) - k_{\mathrm{ref}}^2 \quad (7)$$

The reference quantities were $k_{ref} = k_0 n_0$ and $n_0 = n_{core} = 1.461$. Each propagation step treats diffraction in Fourier space and the index-dependent phase in real space. The transverse grid and refractive-index map are identical to those used for the eigenmode calculation. Propagation was carried out to $z_{max} = 10$ mm in steps of $\Delta z = 1$ μm. Since the Fourier calculation imposes periodicity at the transverse edges, the wide 125 μm window was chosen to limit interaction with those boundaries. A separate test of convergence with window size was not carried out.

2.5. Core power and BPM transfer length

At axial position z, the fraction of the total computed transverse power located inside core j is

$$P_j(z) = \frac{\iint_{\Omega_j} |A|^2 \, dS}{\iint_{\Omega} |A|^2 \, dS} \quad (8)$$

Here Ω_j is the disk occupied by core j, and Ω is the full transverse domain. The BPM coupling length $L_{c,BPM}$ was defined as the position of the first maximum in $P_2(z)$ following excitation of core 1. In Fig. 5, the two traces are displayed as $P_1/(P_1+P_2)$ and $P_2/(P_1+P_2)$. These normalized traces describe the distribution of power within the chosen core disks. They do not account for all field energy in the cladding or in radiation modes. The relative deviation between the two coupling-length estimates is defined by

$$\varepsilon(\%) = 100 \times \left| \frac{L_{c,\mathrm{BPM}} - L_{c,\mathrm{CMT}}}{L_{c,\mathrm{BPM}}} \right| \quad (9)$$

3. Results and discussion

3.1. Effective indices and mode splitting

The fields in Fig. 1 have the parity expected of the two lowest-order supermodes: equal signs in the two cores for the even field and opposite signs for the odd field. Their effective-index branches move closer together with increasing separation (Fig. 2). Figure 3 shows the corresponding decline in Δneff across the four computed geometries. The trend follows the reduction in evanescent overlap as the cores become more widely separated [10–16].

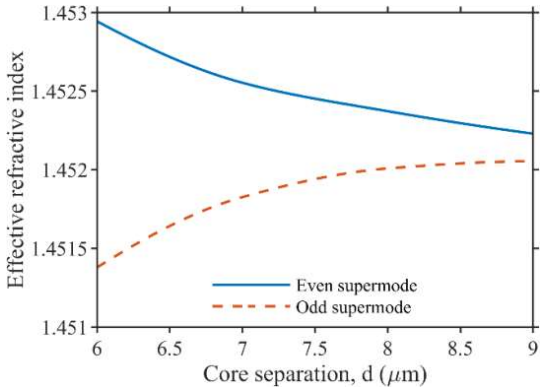


Figure 2. Effective indices of even and odd supermodes versus separation.

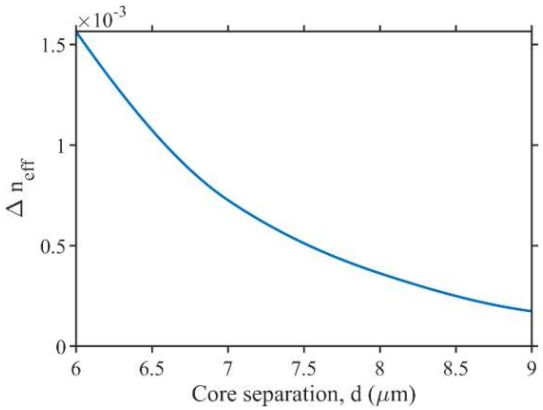


Figure 3. Effective-index splitting Δn_eff versus separation.

Only four discrete separations were computed for the radius, refractive indices, and wavelength stated in Section 2. The connecting lines in Figs. 2 and 3 help show the trend but do not represent additional simulations. In particular, these points cannot be used to infer a general decay constant for other geometries.

3.2. Coupling length from eigenmodes and BPM

The reduction in Δn_{eff} translates into a pronounced increase in transfer length through Eq. (5). Figure 4(a) shows L_c rising from approximately 0.5 mm for d = 6 μm to roughly 4.4 mm for d = 9 μm. This change is expected from weaker field overlap at greater spacing. Four data points, however, do not justify fitting a general exponential law.

The transfer lengths obtained from BPM track the modal predictions closely. At separations of 6, 7, 8, and 9 μm, the relative differences are 0.25%, 0.32%, 0.33%, and 0.61%, respectively (Fig. 4b). All four are below 1%. This comparison concerns the first transfer peak produced by the specified Gaussian input in two scalar calculations; it is not a comparison with experimental data or an independently established full-vector reference.

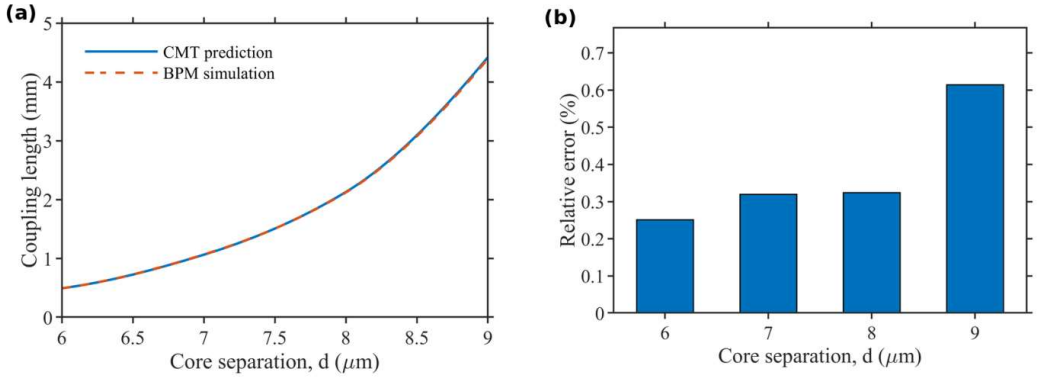


Figure 4. (a) Coupling length obtained from supermode splitting (CMT prediction) and directly from BPM; **(b)** their relative difference.

Figure 4(b) measures agreement between the two numerical descriptions, rather than error against an exact reference. The eigenvalue calculation uses the scalar transverse Helmholtz equation, while BPM follows a paraxial approximation. A Gaussian launch may excite contributions beyond the fundamental supermode pair, and the first transfer maximum is located using a finite axial step. These effects may produce small differences between the coupling lengths. Without separate convergence tests of the transverse grid, longitudinal step, launch conditions, and computational window, those differences cannot be assigned to a single source. What is established is that the beating distance obtained from the modal splitting is also seen in the propagated field.

3.3. Longitudinal power exchange

The variation of coupling length with core spacing is evident in the longitudinal intensity maps of Fig. 5. At d = 6 μm, power passes back and forth between the cores many times within 10 mm. Fewer oscillations fit into that distance at 7 and 8 μm; at 9 μm, there is approximately one dominant transfer cycle. The first peaks of the core-resolved traces provide the BPM lengths used in Fig. 4.

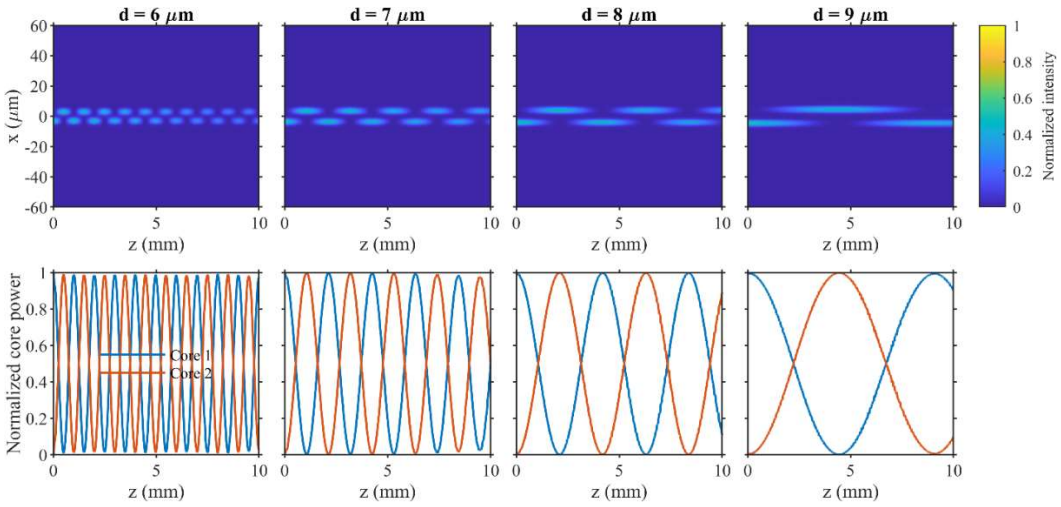


Figure 5. BPM longitudinal intensity maps (top) and relative core-resolved power fractions (bottom) for d = 6, 7, 8, and 9 µm.

A near-unity value in the lower panels of Fig. 5 refers only to the relative power in the two core disks. It means that nearly all power counted within those disks is in one core at that axial position. It does not show that nearly all of the input power has been guided into, or transferred to, that core. An absolute efficiency estimate would also need the total core-disk power $P_1 + P_2$ and preferably a distinction between guided and radiative contributions. Those quantities are not supplied by the normalized traces.

3.4. Scope and numerical limitations

Varying only separation makes its role visible without changes in core size or refractive index. The resulting curves nevertheless apply only to the four geometries considered. Their spacing was chosen to suit the finite propagation window, not to represent fabrication tolerances. The scalar treatment leaves out polarization-dependent behavior, and the incident Gaussian is not itself a guided eigenmode. Also, power integrated over a core disk is not the same as power carried by a particular guided mode. The wide transverse window was intended to reduce boundary interaction with the guided field, but window-size and radiation-boundary tests would be needed before assigning a reliable numerical error bound.

As the even and odd supermodes approach degeneracy, the accuracy of their effective-index difference becomes increasingly sensitive to small errors in the individual eigenvalues. An absolute eigenvalue error may therefore become significant relative to Δn_{eff}. Identification of the even and odd branches was checked through their spatial parity, but this check alone does not establish the accuracy of the splitting. A grid-refinement study would be required for that assessment. The results also

cannot be applied without new calculations to asymmetric, birefringent, bent, nonlinear, or photonic-crystal fibers. Only the specified symmetric structure has been considered in this comparison of two established numerical methods.

4. Conclusion

For the symmetric step-index dual-core fiber considered, increasing the center separation from 6 to 9 μm reduced the splitting of the fundamental supermodes and lengthened the first ideal transfer distance from about 0.5 to 4.4 mm. The coupling lengths obtained from the finite-difference eigenmodes and split-step Fourier BPM differed by 0.25%–0.61% across the four separations. The longitudinal power maps displayed the corresponding change from rapid to slower oscillations. This agreement confirms consistency between the two scalar calculations for the stated geometry and Gaussian launch, but it is not an experimental measurement of transfer efficiency or a validation against a full-vector electromagnetic solution. Convergence tests and other excitation conditions would be needed before extending the findings to more general fiber designs.

Data availability. Numerical data and the MATLAB scripts for Figs. 2–5 is deposited in Zenodo (https://doi.org/10.5281/zenodo.21295600).

References

1. Richardson, D. J., Fini, J. M., & Nelson, L. E. (2013). Space-division multiplexing in optical fibres. *Nature Photonics*, 7, 354–362. https://doi.org/10.1038/nphoton.2013.9
2. Essiambre, R.-J., Kramer, G., Winzer, P. J., Foschini, G. J., & Goebel, B. (2010). Capacity limits of optical fiber networks. *Journal of Lightwave Technology*, 28(4), 662–701. https://doi.org/10.1109/JLT.2009.2039464
3. Saitoh, K., & Matsuo, S. (2016). Multicore fiber technology. *Journal of Lightwave Technology*, 34(1), 55–66. https://doi.org/10.1109/JLT.2015.2466444
4. Puttnam, B. J., Rademacher, G., & Luís, R. S. (2021). Space-division multiplexing for optical fiber communications. *Optica*, 8(9), 1186–1203.https://doi.org/10.1364/OPTICA.427631
5. Chen, W., Yuan, L., Zhang, B., Yu, Q., Lian, Z., Pi, Y., Shan, C., & Shum, P. P. (2024). Applications and development of multi-core optical fibers. *Photonics*, 11(3), 270. https://doi.org/10.3390/photonics11030270
6. Yao, Y., Chen, X., Dai, Y., & Yao, J. (2023). Advances in multicore fiber

interferometric sensors. *Sensors*, 23(7), 3436. https://doi.org/10.3390/s23073436

7. Zhao, Z., Soto, M. A., Tang, M., & Thévenaz, L. (2020). Distributed multicore fiber sensors. *Opto-Electronic Advances*, 3, 190024. https://doi.org/10.29026/oea.2020.190024
8. Su, J., & Biaggio, I. (2022). Dual-core optical fibers for efficient mid-infrared generation via third-order frequency mixing and coupling-length phase matching. *Journal of the Optical Society of America B*, 39(3), 729–741. https://doi.org/10.1364/JOSAB.449934
9. Xiong, C., Wang, C., Yu, R., Ji, W., Qin, Y., Shen, Y., Chen, W., Liu, A.-Q., & Xiao, L. (2024). 3D printed multicore fiber-tip discriminative sensor for magnetic field and temperature measurements. *Light: Advanced Manufacturing*, 5, Article 18. https://doi.org/10.37188/lam.2024.018
10. Snyder, A. W., & Love, J. D. (1983). *Optica*l waveguide theory. Chapman and Hall, London, UK. https://doi.org/10.1007/978-1-4613-2813-1
11. Marcuse, D. (1991). *Theory of dielectric optical waveguides* (2nd ed.). Academic Press, San Diego, CA, USA.
12. Okamoto, K. (2006). *Fundamentals of optical waveguides* (2nd ed.). Academic Press, Amsterdam, The Netherlands.
13. Yariv, A. (1973). Coupled-mode theory for guided-wave optics. *IEEE Journal of Quantum Electronics*, 9(9), 919–933. https://doi.org/10.1109/JQE.1973.1077767
14. Haus, H. A., Huang, W., Kawakami, S., & Whitaker, N. A. (1987). Coupled-mode theory of optical waveguides. *Journal of Lightwave Technology*, 5(1), 16–23. https://doi.org/10.1109/JLT.1987.1075416
15. Hardy, A., & Streifer, W. (1985). Coupled-mode theory of parallel waveguides. *Journal of Lightwave Technology*, 3(5), 1135–1146. https://doi.org/10.1109/JLT.1985.1074291
16. Huang, W.-P. (1994). Coupled-mode theory for optical waveguides: An overview. *Journal of the Optical Society of America A*, 11(3), 963–983. https://doi.org/10.1364/JOSAA.11.000963
17. Puttnam, B. J., Luís, R. S., Agrell, E., Rademacher, G., Sakaguchi, J., Klaus, W., Saridis, G. M., Awaji, Y., & Wada, N. (2017). High capacity transmission systems using homogeneous multi-core fibers. *Journal of Lightwave Technology*, 35(6), 1157–1167. https://doi.org/10.1109/JLT.2017.2669207

18. Rademacher, G., Luís, R. S., Puttnam, B. J., Awaji, Y., & Wada, N. (2017). Crosstalk dynamics in multi-core fibers. *Optics Express*, 25(10), 12020–12028. https://doi.org/10.1364/OE.25.012020
19. Rademacher, G., Luís, R. S., Puttnam, B. J., Ryf, R., van der Heide, S., Eriksson, T. A., Fontaine, N. K., Chen, H., Essiambre, R.-J., Awaji, Y., & Furukawa, H. (2022). A comparative study of few-mode fiber and coupled-core multi-core fiber transmission. *Journal of Lightwave Technology*, 40(6), 1590–1596. https://doi.org/10.1109/JLT.2021.3124521
20. van Uden, R. G. H., Amezcua Correa, R., Lopez, E. A., Huijskens, F. M., Xia, C., Li, G., Schülzgen, A., de Waardt, H., Koonen, A. M. J., & Okonkwo, C. M. (2014). Ultra-high-density spatial division multiplexing with a few-mode multicore fibre. *Nature Photonics*, 8, 865–870. https://doi.org/10.1038/nphoton.2014.243
21. Zou, H., Xu, J., Jiang, M., & Chen, Y. (2024). An excellent super-polarization-independent optical directional coupler based on dual-core photonic crystal fibre with a bandwidth of 390 nm. *Physica Scripta*, 99(6), 065549. https://doi.org/10.1088/1402-4896/ad49da
22. Longobucco, M., Pysz, D., Buczyński, R., & Bugár, I. (2024). Ultrafast dual-wavelength 1 µm–2 µm all-optical switching based on all-solid dual-core fiber. In 2024 24th International Conference on Transparent *Optica*l Networks (ICTON) (pp. 1–4). IEEE. https://doi.org/10.1109/ICTON62926.2024.10647956
23. Zhang, Z., Chen, H., Wang, C., & Li, Y. (2023). A broadband optical fiber coupler based on dual-hollow core fiber. *Journal of Physics: Conference Series*, 2517, 012009. https://doi.org/10.1088/1742-6596/2517/1/012009
24. Zhou, G., Yuan, J.-H., Wang, K., Yan, B., Wu, Q., & Zhou, G. (2024). A polarization beam splitter based on dual hollow-core anti-resonant fiber with high extinction ratio and large bandwidth. In 2024 14th International Symposium on Communication Systems, Networks and Digital Signal Processing (CSNDSP) (pp. 283–286). IEEE. https://doi.org/10.1109/CSNDSP60683.2024.10636581
25. Zhang, K., Zhang, J., Xiao, A., Wang, Y., Ling, Q., Wang, Y., Zhang, Y., Yu, Z., Guan, Z., & Chen, D. (2025). Simultaneous detection of vector bending and temperature using dual-core fiber cascaded FBG structure. *Measurement*, 241, 115760.

https://doi.org/10.1016/j.measurement.2024.115760

26. Zhu, X., Ren, Z., Xu, Q., Zhou, R., Chen, H., Ling, Q., Wang, X., Yu, Z., & Chen, D. (2025). Dual-core fiber-assemble long period fiber grating for vector bending sensing. *Optics and Lasers in Engineering*, 186, 108774. https://doi.org/10.1016/j.optlaseng.2024.108774
27. Xu, R., Li, X., Liu, W., Lv, J., Yang, L., Wang, J., Liu, Q., Chu, P. K., & Liu, C. (2024). Symmetrical dual-D and dual-core single-mode fiber surface plasmon resonance liquid sensor. *Journal of the Optical Society of America A*, 41(8), 1469–1478. https://doi.org/10.1364/JOSAA.525157
28. Feit, M. D., & Fleck, J. A., Jr. (1978). Light propagation in graded-index optical fibers. *Applied Optics*, 17(24), 3990–3998. https://doi.org/10.1364/AO.17.003990
29. Feit, M. D., & Fleck, J. A., Jr. (1980). Computation of mode properties in optical fiber waveguides by a propagating beam method. *Applied Optics*, 19(7), 1154–1164. https://doi.org/10.1364/AO.19.001154
30. Saleh, B. E. A., & Teich, M. C. (2019). *Fundamentals of photonics* (3rd ed.). Wiley, Hoboken, NJ, USA.
31. Zhao, T., Ren, W., Yin, T., & Wang, F. (2021). Calculation of the coupling coefficient of twin-core fiber based on the supermode theory with finite element method. *Optics and Photonics Journal*, 11, 402–411. https://doi.org/10.4236/opj.2021.11802
32. Jin, W., & Jian, S. (2017). Numerical and simulation analyses on supermode characteristics of dual-core fiber and four-core fiber. *Optik*, 132, 32–38. https://doi.org/10.1016/j.ijleo.2016.12.042
33. Wang, Z., Taru, T., Birks, T. A., Knight, J. C., Liu, Y., & Du, J. (2007). Coupling in dual-core photonic bandgap fibers: Theory and experiment. *Optics Express*, 15(8), 4795–4803. https://doi.org/10.1364/OE.15.004795